Formation Mechanism for Stable Hybrid Clusters of Proteins and Nanoparticles

Sebastian T. Moerz,[†] Annette Kraegeloh,[†] Munish Chanana,[‡] and Tobias Kraus*[,†]

[†]INM - Leibniz Institute for New Materials, Campus D2 2, 66123 Saarbrücken, Germany and [‡]Physikalische Chemie II, Universität Bayreuth, 95440 Bayreuth, Germany

ABSTRACT Citrate-stabilized gold nanoparticles (AuNP) agglomerate in the presence of hemoglobin (Hb) at acidic pH. The extent of agglomeration strongly depends on the concentration ratio [Hb]/[AuNP]. Negligible agglomeration occurs at very low and very high [Hb]/[AuNP]. Full agglomeration and precipitation occur at [Hb]/[AuNP] corresponding to an Hb monolayer on the AuNP. Ratios above and below this value lead to the formation of an unexpected phase: stable, microscopic AuNP–Hb agglomerates. We investigated the kinetics of agglomeration with dynamic light scattering and the adsorption kinetics of Hb on planar gold with surface-acoustic wave-phase measurements. Comparing agglomeration and adsorption kinetics leads to an explanation of the complex behavior of this nanoparticle–protein mixture. Agglomeration is initiated either when Hb bridges AuNP or when the electrostatic repulsion between AuNP is neutralized by Hb. It is terminated when Hb has been depleted or when Hb forms multilayers on the agglomerates that stabilize microscopic clusters indefinitely.

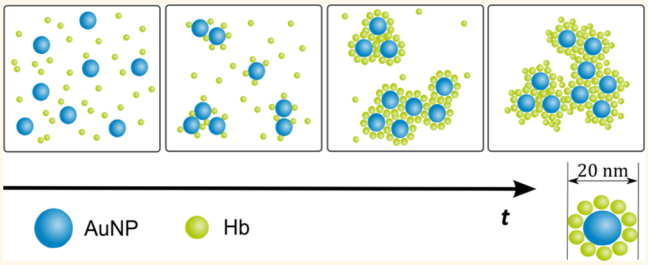

KEYWORDS: agglomeration · clusters · protein corona · time-dependent Smoluchowiski agglomeration model · protein–nanoparticle mixtures · dispersion stability · electrosteric stabilization · particle stability

Proteins interact with dispersed, charged nanoparticles (NP) and act as complex surfactants. Electrostatic, dispersive, and covalent interactions cause proteins to adsorb on NP surfaces and to change their molecular conformation.[1−3] Adsorption can decrease or increase the NPs' colloidal stability: proteins can cause agglomeration when they reduce the NPs' surface charge[4] or directly bind to two NP and bridge them.[5] NP stability can increase if the proteins act as a spacer between the individual particles and cause steric or entropic stabilization.[6−8]

In many applications, NP agglomeration is undesirable, and stable dispersions are required even at the high physiological ionic strength of biological fluids.[9] In other cases, protein-induced NP agglomeration is intended, for example, in immunoassays where NP specifically bind antibodies.[10] The agglomeration of gold nanoparticles (AuNP) can easily be detected photometrically due to a strong shift in the AuNPs' surface plasmon resonance (SPR).[11] Similar concepts have been used to detect metal ions[4] and conformational transitions of proteins.[12]

An interesting intermediate case is that of NP–protein clusters with stable, microscopic sizes. They can form when proteins bridge particles[5] or when agglomeration is deliberately stopped by stabilizing proteins.[8] Here, we are interested in the spontaneous growth of stable NP–protein clusters that occurs without quenching.

The stability of charged colloids is commonly described by the DLVO theory.[13,14] This theory states that a colloidal dispersion is stable when electrostatic repulsion outweighs van der Waals (vdW) attraction and otherwise agglomerates until transport limitations end the process, usually at macroscopic agglomerate sizes. Stable clusters can only form when the agglomeration process is quenched by a secondary process.

Several authors report self-limiting agglomerate growth: Sevilla *et al.*[15] observed stable clusters after mixing equine myoglobin with an unbuffered dispersion of citrate-stabilized 30 nm AuNP. They investigated myoglobin concentrations from 3.7×10^{-8} to 7.4×10^{-6} M (0.65 mg/L to 130 mg/L) at a fixed AuNP concentration and found

* Address correspondence to tobias.kraus@inm-gmbh.de.

Received for review February 13, 2015 and accepted June 1, 2015.

Published online June 01, 2015
10.1021/acsnano.5b01043

smaller agglomerates and faster agglomeration kinetics for higher protein concentration.

In a study by Park *et al.*,[16] 3.8 nm CdTe−NP were found to agglomerate in the presence of cytochrome *c*. They formed microscopic clusters with a narrow monomodal size distribution and zeta potentials that increased with progressing agglomeration until electrostatic repulsion terminated further cluster growth. Similar observations were reported by Kalsin *et al.*[17] for a protein-free system: Polydisperse but finite-sized supracrystals formed in a binary mixture of similar-sized and oppositely charged metal nanoparticles. An excess of either particle type resulted in an asymmetrical composition of the clusters' outermost layer and gave rise to electrostatic stabilization.

We suggest that stable clusters form when repulsive interactions, be they electrostatic, steric, or due to depletion, increase in an unstable colloid until they stop agglomeration and yield stable clusters. There is insufficient kinetic data on cluster growth available to decide in which nanoparticle-protein mixtures such mechanisms lead to stable clusters. An alternative explanation for stable clusters are equilibrium cluster phases[18] that may also occur in nanoparticle-protein mixtures. The intent of the work reported here was to establish a formation mechanism for one representative cluster-forming mixture.

We investigated the agglomeration of citrate-stabilized AuNP in acidic solutions (pH 4) of bovine hemoglobin (Hb) and bovine serum albumine (BSA) solutions. The proteins have similar molecular weights (66.4 kDa for BSA and 64.5 kDa for Hb) and positive net charges at the pH value used in this study (isoelectric point pI 4.9 for BSA and pI 6.8 for Hb). Dynamic light scattering (DLS) indicated agglomerate growth kinetics and agglomerate stability. Surface acoustic wave (SAW) phase measurement was used to analyze Hb adsorption kinetics on planar gold surfaces. Taken together, the kinetic data suggest concentration-dependent mechanisms of agglomeration and cluster formation in this system and exclude equilibrium cluster phases. A modified Smolukowski agglomeration model is introduced to explain the formation of finite-sized clusters in NP-protein mixtures.

RESULTS AND DISCUSSION

To identify the formation mechanism of AuNP−Hb clusters, we measured time- and concentration-dependent cluster sizes, assessed the stability of the formed clusters upon addition of protein, and characterized the adsorption kinetics of Hb on gold *ex situ*. This data allows us to model the transient stability of AuNP−Hb agglomerates and forms the basis of a modified Smulochowski agglomeration model that describes the formation of stable clusters.

Cluster Radius *versus* Hemoglobin Concentration. The size distribution of AuNP−Hb clusters depended on the ratio of Hb and AuNP concentrations, [Hb]/[AuNP]. Mixtures were prepared with a AuNP concentration of 16.15 mg/L (measured by ICP-OES) and different Hb concentrations. Protein-free samples were red due to surface plasmon resonance (SPR) of the AuNP. DLS indicated a particle radius of 7.3 ± 1.0 nm, consistent with the observed color.[11]

Within minutes after mixing AuNP and Hb, samples with Hb concentrations in the range of 0.2−10 mg/L changed their color from red to violet, probably due to the SPR coupling upon particle agglomeration[4,11,19] (see Figure 1a). After a few hours, samples with concentrations between 0.5 and 5 mg/L Hb further changed color to dark blue. Mixtures in this concentration range precipitated within 1 day and left an almost colorless clear liquid (Figure 1a). We call this concentration range the "instability region". Note that the Hb concentration theoretically required to form a complete monolayer on the AuNP lies between 3.3 and 4.1 mg/L (Supporting Information), clearly inside the instability region.

Samples with Hb concentrations above 5 mg/L underwent no or hardly noticeable precipitation and a SPR red-shift that decreased monotonically with increasing Hb concentration (UV−vis spectra in the Supporting Information Figure S1). Samples with Hb concentrations below 0.5 mg/L exhibited the inverse trend: SPR red-shift and precipitation decreased with decreasing protein concentrations.

The surface plasmon shifts in the stable dispersions are likely due to the formation of stable, microscopic clusters. We used DLS to quantify the agglomeration. At very high and very low Hb concentrations, no agglomeration occurred, and DLS measured the radii of single particles. Stable clusters formed at Hb concentrations below 0.5 and above 5 mg/L. Mean radii of stable clusters that had formed after 24 h at different Hb and constant AuNP concentrations are shown in Figure 1b. The error bars indicate the cluster size distributions calculated from the averaged autocorrelation functions.

Clusters that formed outside the instability region at moderate Hb concentrations were stable and did not show significant changes even after hundreds of hours as shown in Figure 1c for a sample prepared with 25 mg/L Hb. We reproduced the results shown in Figure 1b with four different AuNP batches and different buffer dilutions (Supporting Information, Figures S2 and S3).

Replacing Hb with BSA resulted in very similar agglomeration behavior (Supporting Information, Figure S4). We will focus on hemoglobin in the rest of this study but suggest that stable AuNP agglomerates form with many other proteins.

The relationship between concentration and agglomerate sizes observed is similar to that reported by Sevilla *et al.*[15] and Kalsin *et al.*[17] in a nonprotein system. Kalsin observed diverging cluster sizes when using

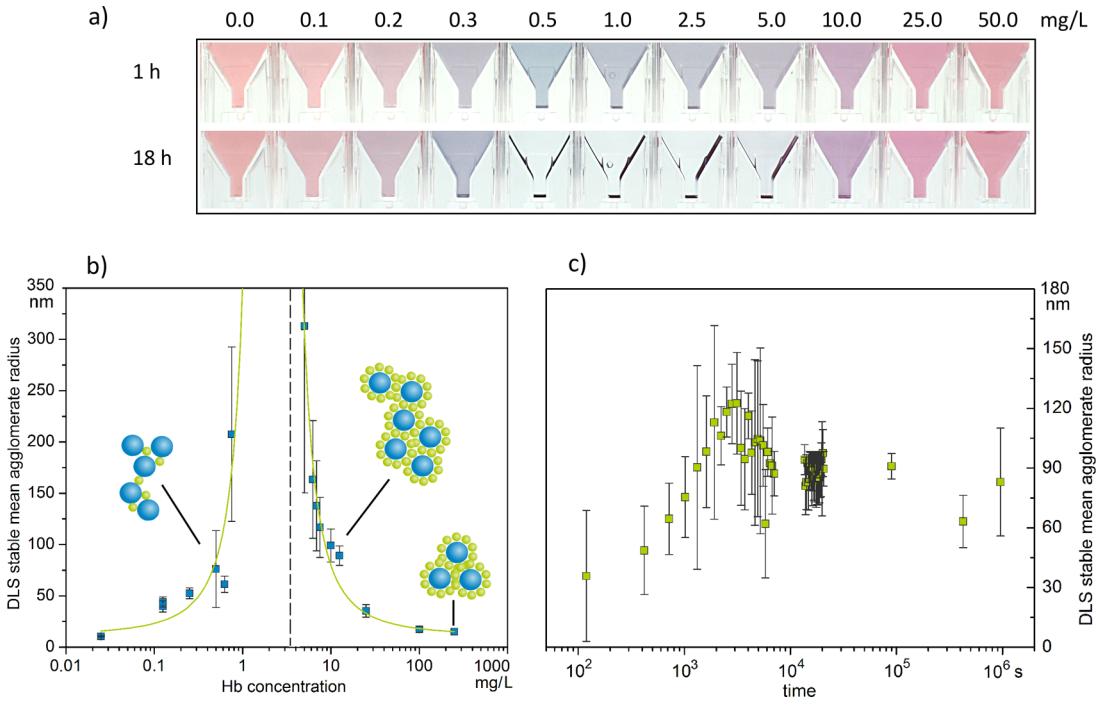

Figure 1. (a) Photographs of particle−protein mixtures containing 16.15 mg/L AuNP after 1 h (top row) and 18 h (bottom row). Hemoglobin (Hb) concentrations were (from left to right) 0, 0.1, 0.2, 0.3, 0.5, 1, 2.5, 5, 10, 25, and 50 mg/L. (b) Mean agglomerate radii of stable AuNP clusters from DLS as a function of Hb concentration at a constant AuNP concentration of 16.15 mg/L. The samples were prepared approximately 24 h before the measurement. Error bars indicate the size distributions calculated from DLS. The green line is a guide to the eye. The Hb concentration theoretically required for monolayer coverage of the AuNP is indicated as a vertical dashed line. Blue spheres represent AuNP, green spheres represent Hb, and both are not to scale. (c) Long-term evolution of the mean agglomerate radii from DLS in clusters formed at 16.15 mg/L AuNP and 25.0 mg/L Hb. Error bars indicate size distributions from DLS.

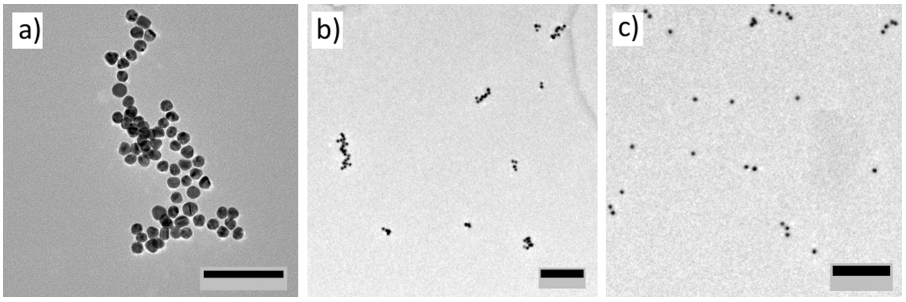

Figure 2. Transmission electron micrographs of agglomerated AuNP for different Hb concentrations: (a) 9.125 mg/L Hb, (b) 20.0 mg/L Hb, (c) 75.0 mg/L. The scale bars are 100 nm in (a) and 200 nm in (b) and (c).

identical concentrations of negatively and positively charged nanoparticles and a strong decrease in cluster radii when the concentration of either particle type was increased.

Transmission electron microscopy (TEM) of agglomerates prepared outside of the instability region showed floclike agglomerates and confirmed the decrease in cluster size with rising Hb concentration (Figure 2). The clusters were polydisperse for all concentrations, with a disordered geometry consistent with diffusion-limited agglomeration.[8,20] This is in contrast to the almost monodisperse agglomerates found by Park *et al.*[16] and the crystalline suprastructures found by Kalsin *et al.*[17]

Cluster Stability upon Dilution and Protein Addition. Statistical models that use kinetic constants to describe the adsorption and desorption of particles on agglomerates predict that stable clusters can form in a dynamic equilibrium.[21] Dynamic equilibrium implies a strong dependence of the agglomerate radius on the absolute particle concentrations. A low particle concentration will reduce the rate of Brownian collisions of free particles with the cluster and thus, the adsorption rate, while the desorption rate is independent of the absolute particle concentration. Dilution should therefore reduce the equilibrium cluster size.

Molecular dynamic simulations that attribute interaction potentials to the particles (for example, Lennard-Jones and Yukawa potentials) also predict stable clusters for certain parameter ranges.[18] Park *et al.* use such a model to explain the nanoparticle clusters they

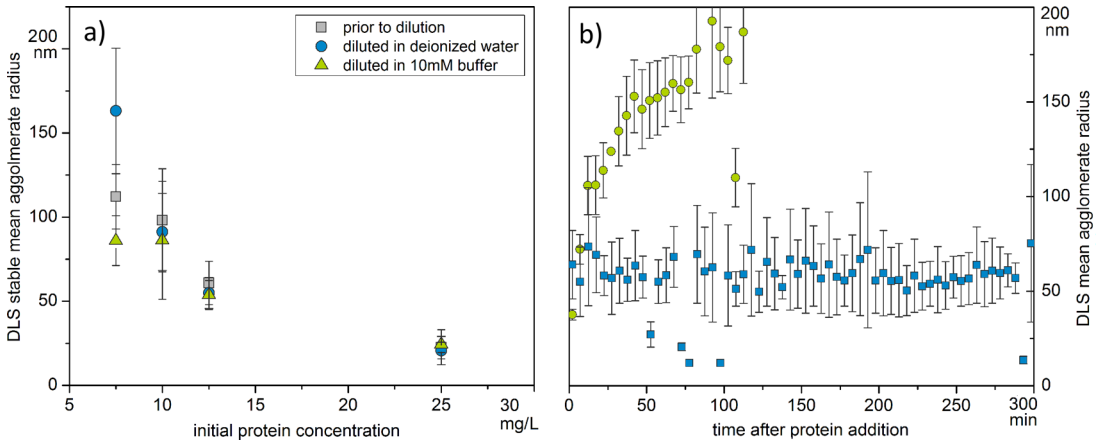

Figure 3. Stability of Hb−AuNP clusters in pH 4.0 buffer measured by DLS. AuNP concentration was 16.15 mg/L; error bars indicate cluster size distributions. (a) Mean radius of clusters prepared at Hb concentrations above the instability region after 24 h (gray squares). The samples were diluted with deionized water (blue circles) or pH 4.0 buffer (green triangles) and characterized after another 24 h. (b) Stability after protein addition of clusters prepared on either side of the instability region with initial Hb concentrations of 12.5 mg/L (blue squares) and 0.25 mg/L (green circles).

observe: Initial formation of large agglomerates is followed by a slow condensation into an equilibrium phase of compact, electrostatically stabilized clusters.[16]

All of the dynamic equilibrium models described above predict cluster sizes that change upon dilution. We tested whether the cluster sizes are concentration-dependent in our system. A volume of 200 μL dispersion of stable clusters was diluted with 800 μL of either deionized water or pH 4.0 buffer. Diluting did not change the color of the dispersion and did not cause any visible precipitation. The mean cluster radius was measured 24 h after the samples were diluted using four protein concentrations above the instability region (Figure 3a). Cluster sizes and size distributions remained constant after dilution for initial Hb concentrations of 10 mg/L and higher. Clusters formed at 7.5 mg/L Hb, close to the instability region, changed their size upon dilution by a factor of 1.5. We also measured the hydrodynamic radius upon cluster formation at different absolute concentrations with identical [Hb]/[AuNP] (Supporting Information, Table 1). Low absolute concentrations yielded the largest clusters. Overall, the concentration dependence of cluster sizes that we observed cannot be explained using dynamic equilibrium models that would predict smaller clusters at lower concentrations. We believe that kinetics dominate the cluster sizes.

While dilution changed the absolute gold and protein concentrations, their ratio remained constant. We additionally changed [Hb]/[AuNP] by adding highly concentrated Hb solutions to stable cluster dispersions. Figure 3b shows the time evolution of the mean radii of clusters prepared on either side of the instability region. Clusters formed at high initial Hb concentration (12.5 mg/L) retained their mean radius after increasing the Hb concentration to 37.5 mg/L. Clusters formed at low Hb concentrations (0.25 mg/L) agglomerated upon increasing the Hb concentration to 3.25 mg/L and eventually precipitated.

The observed differences suggests different stabilization mechanisms for clusters formed at protein concentrations above or below the instability region. At low concentrations, stability is probably due to the depleting of proteins from the solution by the growing clusters. Proteins adsorbed to (and inside) the clusters do not further contribute to particle agglomeration. When all proteins are depleted, the partially protein-coated clusters remain stable (see the illustration in Figure 1b). When we added proteins to such clusters, agglomeration resumed until the additional protein was consumed. This reminds of the mechanism proposed by Bharti *et al.* for the agglomeration of silica nanoparticles in lysozyme solutions[5,22] and is different from the mechanism suggested by Kalsin *et al.*[17]

Clusters formed at protein concentrations above the instability region must be stabilized by different mechanisms. We suggest (see Figure 1b) that such clusters are fully coated by layers of proteins that provide polymer stabilization of the clusters.[23] Such clusters are not affected by additional proteins.

According to the above model, clusters will grow either until no proteins remain in the solution or until a protein layer has formed on the clusters that stabilizes them against further growth. Cluster sizes would then depend on the kinetics of protein adsorption.

Kinetics of Hemoglobin Adsorption on Gold Surfaces. We studied the adsorption of Hb on gold in more detail to understand its kinetics and introduce it to a possible model of cluster formation. The surface acoustic wave shift of a planar gold film was monitored during protein adsorption. Phase shifts that occurred at different Hb concentrations in diluted pH 4.0 buffer are shown in Figure 4a. The temporal evolution of the shift (that is proportional to surface-bound mass) indicates a two-step process as previously reported for Hb on gold.[3] Monte Carlo simulations of a similar case, the adsorption of α-amylase and BSA on silicon substrates,

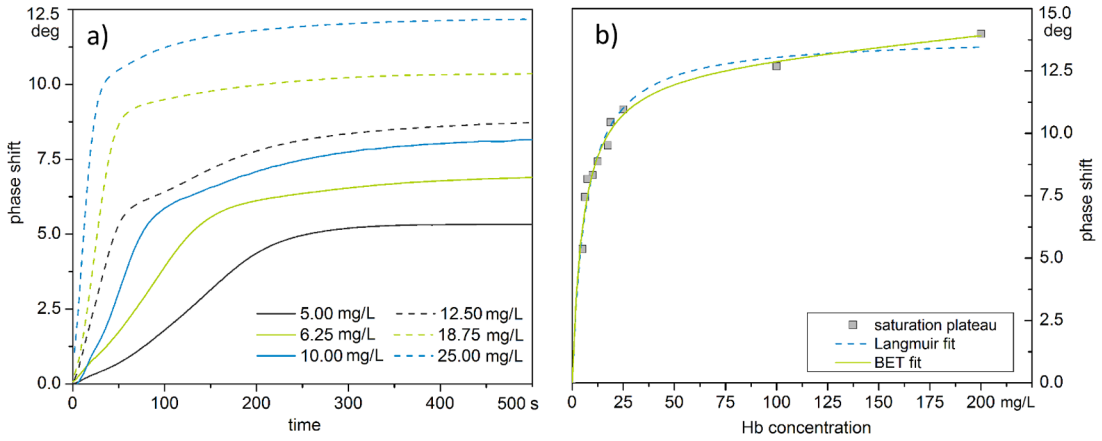

Figure 4. SAW data of hemoglobin adsorption on a planar gold film. (a) Phase shift of the surface acoustic wave *vs* time after sample injection for different Hb concentrations. For better visibility, not all data are shown in this plot. See text for discussion. (b) Saturation value of the phase shift *vs* Hb concentration. The data are fitted to the Langmuir (blue dashed line) and the BET (green solid line) adsorption isotherms. Parameters of the Langmuir fit are θ_{mono} = 13.9° ± 0.4°, α_L = 0.15 ± 0.02L/mg. Parameters of the BET fit are θ_{mono} = 12.9° ± 0.7°, α_{BET} = 386 ± 205, C_0 = 2081 ± 1373 mg/L.).

suggest that after the primary protein adsorption slower conformational changes of the adsorbed protein increase packing density.[1] Circular dichroism spectroscopy reveals strong changes in the secondary structure of Hb adsorbed to gold surfaces, showing that conformational changes indeed happen during Hb adsorption.[24]

We used a linear superposition of two exponentials to fit the time-dependent phase shift $\theta(t)$:

$$\theta(t) = \theta_0 + \theta_{max}(1 - be^{-t/\tau_{SAW,1}} - (1 - b)e^{-t/\tau_{SAW,2}}) \quad (1)$$

Here, θ_{max} is the phase shift for an equilibrated protein layer and θ_0 is the phase shift offset. The time scales of the distinct processes (adsorption and conformational change) are denoted as $\tau_{SAW,1}$ and $\tau_{SAW,2}$. The scaling parameter b describes the relative magnitude of the phase shift attributed to the distinct processes ($1 \geq b \geqslant 0$).

Note that eq 1 fails to describe the initial slope of adsorbed protein mass for Hb concentrations below 10 mg/L. We believe that protein depletion in the small sample cell of the SAW setup causes the deviation from the simple model. Molecules adsorb faster to the uncovered gold surface than they are replenished by the flowing solution. The data are truncated at the inflection point of the initial slope before fitting to eq 1. (See Figure 5 in the Supporting Information for the fits.)

The time scale of the primary adsorption process, $\tau_{SAW,1}$, decreased almost monotonically with increasing protein concentration (Table 1). The time scale of the protein reorganization, $\tau_{SAW,2}$, is approximately 1 order of magnitude larger and almost independent of the Hb concentration, as expected.

Hemoglobin Layer Structure. Cluster stability depends on the structure of adsorbed hemoglobin layers. We used the SAW data to analyze the structure of protein

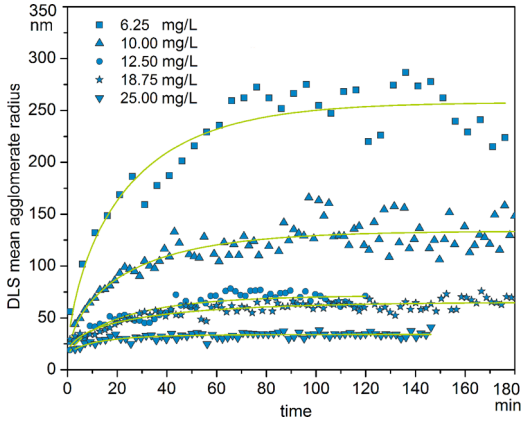

Figure 5. Mean agglomerate radius from DLS *versus* time after sample preparation. The gold concentration was fixed (16.15 mg/L AuNP); Hb concentrations are indicated in the graph (6.25, 10.0, 12.5, 18.75, 25.0 mg/L). Green lines are fits to the modified Smolukowski model (eq 7).

TABLE 1. Fit Parameters Extracted from SAW Data[a]

C_{Hb} (mg/L)	$\theta_0 + \theta_{max}$ (deg)	b	$\tau_{SAW,1}$ (min)	$\tau_{SAW,2}$ (min)	θ_{res} (deg)
5.00	5.36	1	1.0	N/A	4.85
6.25	7.44	0.79	0.79	7.23 ± 1.47	6.53
7.50	8.17	0.55	0.54	2.95	7.62
10.00	8.33	0.52	0.33	2.45	7.79
12.50	8.87	0.52	0.16	2.27	8.35
17.50	9.52	0.67	0.34	2.75	8.88
18.75	10.44	0.85	0.24	2.57	9.7
25.00	10.96[b]	0.78[b]	0.20[b]	2.30[b]	10.3[b]
100.0	12.67[b]	0.89[b]	0.10[b]	2.35[b]	12.1[b]
200.0	13.98	0.88	0.07	2.52	13.34

[a] The saturation value $\theta_0 + \theta_{max}$ of phase shift, the weighing parameter b, and the time constants $\tau_{SAW,1}$ and $\tau_{SAW,2}$ are obtained from eq 1. The residual phase shift after desorption θ_{res} is obtained from an empirical fit (Supporting Information, eq 3). Errors in $\tau_{SAW,1}$ are smaller than 0.02 min; errors in $\tau_{SAW,2}$ are smaller than 0.2 min unless stated otherwise. [b] Average of two independent measurements.

layers formed at different concentrations. The sorption isotherm in Figure 4b shows the phase shift saturation plateau ($\theta_0 + \theta_{max}$) as a function of the sample's hemoglobin concentration. We assume the phase shift signal to be proportional to the mass of the adsorbed protein layer and fit the data with the Langmuir and the BET isotherm (see the Supporting Information for a discussion of the isotherm models).

Both models yield reasonable fits, with slightly smaller deviations from the BET model at higher concentrations. Protein adsorption on AuNP has been reported to deviate from simple Langmuir adsorption previously.[3,25] It is likely that hemoglobin forms at least partial multilayers already at the comparatively low protein concentrations used here.[26]

Multilayer formation explains why the BET isotherm provides the best fit of our protein adsorption data (Figure 4). We suggest that proteins weakly bind to the strongly bound monolayer, in analogy to the classical protein corona picture.[27] Such adsorption is best described by BET even if the underlying monolayer is incomplete.[28] Patches of multilayers will have a minor effect on the overall zeta potential (Supporting Information, Figure S6) but act as a spacer between the agglomerates and suppress attractive interactions.

The adsorption behavior did not change with pH and did not depend on the presence of citrate on the gold surface (Supporting Information, Figure S7). After the protein-coated gold surface was flushed with buffer, over 90% of the original coverage remained irreversibly bound. We believe that similar to other proteins Hb replaces the citrate and forms strong (multivalent) bonds with the gold substrate.[4,6,19] Stable binding of Hb to gold surfaces has been reported in studies that used fluorescence spectrometry.[24,29] Proteins in general have various functional groups, such as carboxylates, amines, thiols, disulfides, and imidazoles that can strongly bind to metal (gold) surfaces, resulting in very robust protein layers.[4] Thiol binding *via* a Cysteine residue is commonly assumed for Hb[3] and other sulfur-containing proteins[12,30] although noncovalent binding *via* tryptophan residues has also been proposed.[24] We suggest that the irreversibly bound proteins are in direct contact with the gold surface where they form at most a monolayer, a notion that is consistent with the literature. The 10% that desorb during flushing were weakly bound in multilayers.

Kinetics of Cluster Growth: Extended Smoluchowski Agglomeration Model. Agglomeration of AuNP at high ionic strengths[8] or after ligand exchange[20] follows the Smoluchowski model of diffusion-limited agglomeration.[31] The total agglomerate concentration $\sum_j[P_j]$ follows a differential equation:[32]

$$-\frac{d}{dt}\sum_j [P_j] = \frac{k}{2}\left(\sum_j [P_j]\right)^2 \quad (2)$$

Here, P_j is the number of agglomerates consisting of j single particles and k is the agglomeration rate constant. The solution

$$\sum_j [P_j] = \frac{P_0}{1 + k/(2P_0)t} \quad (3)$$

describes the kinetics of agglomeration, where the initial particle number is given by the boundary condition $P_0 = \sum_j[P_j]|_{t=0}$.

Equation 3 describes the standard case of unlimited agglomeration. It does not predict the formation of stable clusters for any choice of parameters. In the following, we extend the Smoluchowski model by introducing a time-dependent agglomeration rate. Assume an exponentially decaying agglomeration constant:

$$k(t) = k_0 e^{-t/\tau_{DLS}} \quad (4)$$

(A physical motivation for this choice of time dependence of the agglomeration constant is given in the Supporting Information.) We solve Smoluchowski's eq 2 with this time-dependent $k(t)$ and the boundary condition $P_0 = \sum_j [P_j]|_{t=0}$ and obtain

$$\sum_j [P_j] = \frac{P_0 e^{t/\tau_{DLS}}}{1 + k_0 \tau_{DLS} P_0 (e^{t/\tau_{DLS}} - 1)} \quad (5)$$

The mean particle number $n(t)$ per agglomerate follows as

$$n(t) = \frac{P_0}{\sum_j [P_j]} = (1 - e^{-t/\tau_{DLS}}) k_0 \tau_{DLS} P_0 + e^{-t/\tau_{DLS}} \quad (6)$$

It is easily confirmed that $n(t) = 1$ for $t = 0$ and $n(t) = k_0\tau_{DLS}P_0$ for $t \rightarrow \infty$. Equation 6 also predicts termination of agglomerate growth: if $k_0 \cdot \tau_{DLS} < 1$, $n(t)|_{t=\infty} < P_0$; *i.e.*, the agglomeration stops before all single particles are consumed and bound in one large cluster.

The agglomerate radius R_{agglo} is related to n *via* $n = (((R_{agglo})/(r_0)))^{d_f}$ with the fractal dimension d_f of the agglomerate's geometry and the single AuNP radius r_0. We define a mean agglomerate radius as a function of time:

$$R_{agglo}(t) = ((1 - e^{-t/\tau_{DLS}}) k_0 \tau_{DLS} P_0 + e^{-t/\tau_{DLS}})^{1/d_f} r_0 \quad (7)$$

We used this model to fit time-dependent agglomerate sizes measured by DLS (Figure 5) at five protein concentrations above the instability region. The green lines represent the fits to eq 7, and the fit parameter values are listed in Table 2. All samples exhibited rapid cluster growth after sample preparation and stabilization of cluster sizes within approximately 2 h. Later, agglomeration was entirely suppressed, and the formed clusters remained stable for days as shown in Figure 3.

For all fits shown here, the primary particle radius r_0 was fixed to 10.5 nm, the sum of the AuNP radius of

7.3 nm and a protein radius of 3.2 nm.[33] Initial particle concentrations P_0 were fixed to 5.0125×10^{14} L^{-1}. We adjusted τ_{DLS}, k_0, and d_f. The values of d_f for large agglomerates found here are in reasonable agreement with previously reported values of the fractal dimension for diffusion limited agglomeration of AuNP (d_f = 1.86 and d_f = 2.1−2.2, respectively[8,20]). Note that d_f found for small agglomerates is higher (we chose 3 as upper boundary), as expected for compact structures.

The fits indicate that the time scale of cluster stabilization τ_{DLS} (Table 2) is much shorter than the adsorption of a complete protein film (Table 1). This is surprising at first: if protein adsorption alone governs cluster stabilization, why should there be an additional time scale? One might suggest that our *ex situ* adsorption measurements using SAW overestimate the protein adsorption rate due to the differences in protein diffusion. A quick calculation (in the Supporting Information) confirms, however, that Hb diffusion is much faster than cluster formation even around AuNP.

Measurements of the zeta potential during cluster growth also suggest that protein layers form rapidly. The zeta potential of the clusters increased to slightly positive values around +15 mV (Supporting Information, Figure S6b) almost immediately after sample preparation and remained constant afterward. This surface charge is below the zeta potential of around ±30 mV required to stabilize particles electrostatically.[34]

TABLE 2. Fit Parameters Extracted from the DLS Data Shown in Figure 5[a]

C_{Hb} (mg/L)	k_0 (10^{-15} L/min)	d_f	τ_{DLS} (min)	R_{max} (nm)
6.25	27.4 ± 35.5	2.0 ± 0.5	39.5 ± 12.1	244.5
10.00	9.4 ± 8.0	2.0 ± 0.4	36.7 ± 9.3	138.1
12.50	2.2 ± 1.5	1.9 ± 0.5	31.4 ± 9.6	67.8
18.75	9.4 ± 6.1	3	50.7 ± 12.5	65.2
25.00	3.4 ± 6.4	3	19.7 ± 6.8	33.9

[a] The finite cluster size was calculated as $R_{max}=(k_0\tau P_0)^{1/d_f} r_0$.

We believe that an additional mechanism is relevant in the stabilization of the growing clusters, a mechanism that is slower than protein monolayer adsorption. The stabilization of AuNP by Hb is probably due to steric effects similar to that reported for BSA on AuNP[7] and metal oxide nanoparticles.[9] Protein multilayers seem to be required for efficient stabilization of the clusters. The time scale of multilayer formation is not visible in the SAW measurements because the multilayers contribute only a small fraction (probably around 10%) to the total adsorbed protein mass.

Our modified Smulochowski model does not consider protein multilayer formation explicitly. It is still sufficient to describe the kinetic situation here because the fit parameter k_0 summarizes such effects. Small Hb concentrations will cause slow monolayer formation and protract the transient stage where the energy barrier V_{max} is lowest. At this stage, rapid agglomeration takes place. This is consistent with the decrease of k_0 at increasing Hb concentrations (Table 2 and Supporting Information, Table 1).

A Model for Self-Terminated AuNP Agglomeration. Overall, the following model for the formation of stable finite-sized agglomerates at high protein concentrations emerges (Figure 6): Agglomeration is initiated by the fast adsorption of charged proteins on AuNP that form a strongly bound monolayer. This reduces electrostatic repulsion between individual AuNP and causes diffusion-limited agglomeration. Further protein adsorbs on the growing clusters and forms partial multilayers. Protein multilayers act as spacers between the gold cores and decrease van der Waals attraction. Multilayers reduce attractive interactions until the moderate surface charges (see the Supporting Information, Figure S6) can stabilize the clusters electrostatically, similar to the stabilization mechanism for AuNP:BSA reported by Strozyk *et al.*[19] The time-evolution of cluster stabilization is determined by the time scale of the multilayer growth *via* equation and 7 and the Supporting Information, eq 8. Cluster sizes are

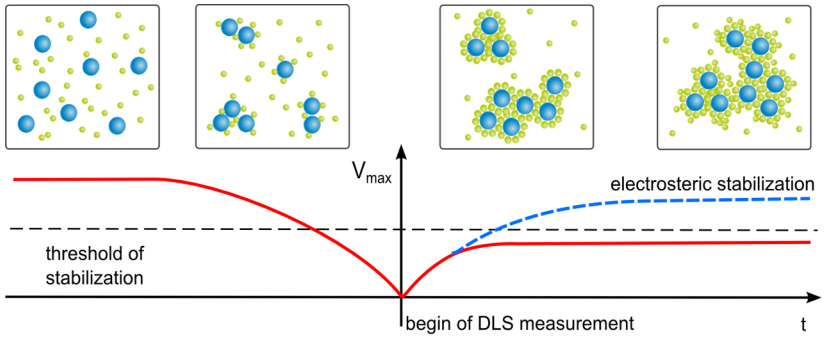

Figure 6. Current model of cluster formation. Adsorption of charged molecules changes the interaction potential maximum V_{max}. At intermediate surface coverage, electrostatic repulsion vanishes and the particles start to agglomerate. The zeta potential (and, thus, V_{max}) increases as further protein adsorbs but saturates below the threshold for electrostatic stabilization (red line). Only partial multilayers can stabilize the agglomerates and quench agglomeration (blue dashed line). The quantitative connection between V_{max} and the agglomeration rate is discussed in the Supporting Information.

determined by τ_{DLS} and the initial value k_0 of the agglomeration rate constant.

At low protein concentrations, the depletion of free proteins limits cluster growth. Small protein patches, possibly down to single proteins, bridge AuNPs.[5] Clusters with low protein content grow until the protein concentration has dropped such that bridging cannot continue. The outer surface of the clusters is made up from citrate-coated AuNP that lend stability to the agglomerate.

CONCLUSIONS

The agglomeration of citrate-stabilized gold nanoparticles (AuNP) in hemoglobin (Hb) solutions was investigated. Depending on the concentration ratio [Hb]/[AuNP], the mixture remained stable, agglomerated and precipitated, or formed stable dispersions of hybrid AuNP:Hb clusters.

Concentration ratios corresponding to a Hb monolayer on the AuNP led to agglomeration and precipitation. No agglomeration occurred for very high and very low [Hb]/[AuNP]. Intermediate values yielded microscopic, nonprecipitating agglomerates or "clusters". The clusters reached their final size within 2 h after mixing. We observed their growth by dynamic light scattering and analyzed the results using a modified Smoluchowski agglomeration model of a diffusion-limited process with an agglomeration rate constant that decays exponentially.

Cluster formation is tightly connected to the adsorption of Hb on AuNP surfaces. We used surface acoustic wave phase measurements to analyze concentration-dependent adsorption on planar gold surfaces. We find two time scales of Hb layer formation, one due to initial protein adsorption and the second (slower) due to molecular reorganization. The BET sorption model fits the adsorption isotherms, indicating at least partial multilayers that Hb forms on top of strongly bound monolayers. Agglomeration stops when such layers form.

We suggest that agglomeration is initiated either (at low [Hb]/[AuNP]) by particle bridging or (at high [Hb]/[AuNP]) by electrostatic destabilization from the oppositely charged Hb. Sufficiently low [Hb]/[AuNP] lead to depletion of Hb, which stops the agglomeration process and leaves clusters. Sufficiently high [Hb]/[AuNP] lead to the formation of Hb multilayers. Such multilayers stabilize particles and clusters electrosterically.

This mechanism is simple enough to be conceivable for many particle−protein combinations. It may be that microscopic, Brownian agglomerates are more common than previously thought. This would be important, for example, in estimating ecological effects of nanoparticle release in aquatic ecosystems or the distribution of nanoparticles in the human body.

METHODS

Synthesis of Gold Nanoparticles. Gold nanoparticles (AuNP) were synthesized using the method first published by Frens.[35] Chloroauric acid ($HAuCl_4$) (45 mg) was dissolved in 20 mL of deionized water (Milli-Q, Merck Chemicals GmbH, Schwalbach, Germany). The solution was filtered through a 0.22 μm regenerated cellulose syringe filter to remove any macroscopic impurities. Deionized water (380 mL) was added to the filtered solution, and the mixture was heated to the boiling point. Subsequently, 14 mL of filtered (0.22 μm RC syringe filter) 1 wt % solution of trisodium citrate was added, and the temperature was kept at the boiling point for another 30 min before the mixture was allowed to cool to room temperature. The solution was stirred at high speed (250−500 rpm) throughout the synthesis.

Sample Preparation. Bovine hemoglobin and bovine serum albumin (products number A2500 and A7030, Sigma-Aldrich Chemie GmbH, Taufkirchen, Germany) were used as received without further purification. Titrisol pH 4.00 buffer concentrate (VWR International GmbH, Darmstadt, Germany) was prepared according to the provided instructions. The buffer was further diluted 1:15 with deionized water to reduce the ionic strength (final concentration of the buffer's components: 0.785 g/L citric acid, 0.299 g/L NaOH, 0.107 g/L HCl).

Protein solutions were freshly prepared with deionized water for each set of experiments and filtered through a 0.22 μm syringe filter to remove macroscopic impurities and undissolved protein.

Samples were prepared by filling a sterile disposable UV−vis cuvette (UVette, Eppendorf AG, Hamburg, Germany) with 100 μL of buffer (diluted as described above) and 50 μL of protein solution. Proper mixing was assured by repeatedly aspirating with the pipet before 50 μL of filtered Au−NP dispersion was added. Larger samples were prepared with the same procedure using multiples of these volumes.

Particle Characterization. The hydrodynamic radius of AuNP and AuNP clusters was measured using dynamic light scattering (DLS). We used a DynaPro Titan (Wyatt Technology Europe GmbH, Dernbach, Germany) at a laser wavelength of 831.2 nm. The laser power was adjusted prior to each measurement to ascertain good count statistics. Sample cell temperature was kept at 25 °C. Autocorrelation functions were averaged from six individual consecutive measurements with an acquisition time of 10 s each. The particle size distribution of the sample was calculated from the first and second cumulant term of a polynomial fit to the averaged autocorrelation curves.[36] If cumulants of higher order are neglected, the particle size distribution is approximated as a Gaussian truncated at zero. The first two cumulants then represent the center and the standard deviation of the distribution.

UV−vis spectra were recorded with an HR2000+ high-resolution spectrometer (Ocean Optics GmbH, Ostfildern, Germany) using a DH-2000-BAL deuterium−halogen light-source (Mikropack GmbH, Ostfildern, Germany) and appropriate fiber optics. The final spectra were averaged from a set of 10 individual spectra with a integration time of 100 ms each and smoothed with a boxcar width of 5.

Transmission electron micrographs (TEM) were recorded with a JEM-2010 microscope (JEOL Germany GmbH, Munich) operated at an accelerating voltage of 200 kV. The samples were diluted 10-fold in deionized water prior to recording the TEM images.

Gold concentrations in the particle dispersions were determined by ICP-OES (Horiba Jobin Yvon Ultima2, HORIBA Jobin Yvon GmbH, Unterhaching, Germany), vaporizer flow rate 0.82 L/min, detection wavelength 242.795 nm). Zeta potential measurements were performed using a Zetasizer Nano (Malvern Instruments GmbH, Herrenberg, Germany).

Surface Acoustic Wave Measurements. Protein adsorption on gold surfaces was measured *via* the phase shift of the surface

acoustic wave of a planar gold surface. We assume that the phase shift is proportional to the adsorbed protein mass. The gold surface was a SAM X biosensor (SAW Instruments GmbH, Bonn, Germany) with unmodified gold-coated sensor chips (providing four individually addressable flow channels per chip). Prior to each experiment, the sensor chip was cleaned in oxygen plasma for 5 min. Titrisol buffer was diluted as described above and used as a running buffer. We allowed the system to equilibrate at a buffer flow of 100 μL/min to saturate the surface with citrate before injection of the protein solutions and mimic the surface chemistry of the citrate-capped nanoparticles. For each concentration, sample aliquots of 300 μL were injected through a single channel at a flow rate of 30 μL/min. Each channel was only used for one single injection to avoid artifacts from residual protein.

Conflict of Interest: The authors declare no competing financial interest.

Acknowledgment. This project was financially supported by INM. Valuable discussions with Inna Dewald and Olga Isakin, University Bayreuth, and Henrike Peuschel, INM, are gratefully acknowledged. We thank Eduard Arzt for his continuing support, Christian Cavelius for zeta potential measurements, Yannic Heider for assistance with UV−vis spectroscopy, Andrea Jung for ICP-OES measurements, Thomas Kister for TEM measurements, Anika Kleemann for particle synthesis, and Ingrid Weiss and Anna Pohl for help with SAW phase measurements.

Supporting Information Available: Figures S1−S7, Table S1, and supporting discussions. The Supporting Information is available free of charge on the ACS Publications website at DOI: 10.1021/acsnano.5b01043.

REFERENCES AND NOTES

1. Schmitt, Y.; Hähl, H.; Giow, C.; Mantz, H.; Jacobs, K.; Leidinger, O.; Bellion, M.; Santen, L. Structural Evolution of Protein-Biofilms: Simulations and Experiments. *Biomicrofluidics* **2010**, *4*, 032201.
2. Moerz, S. T.; Huber, P. Protein Adsorption into Mesopores: A Combination of Electrostatic Interaction, Counterion Release, and van der Waals Forces. *Langmuir* **2014**, *30*, 2729–2737.
3. Jin, B.; Bao, W.-J.; Wu, Z.-Q.; Xia, X.-H. In Situ Monitoring of Protein Adsorption on a Nanoparticulated Gold Film by Attenuated Total Reflection Surface-Enhanced Infrared Absorption Spectroscopy. *Langmuir* **2012**, *28*, 9460–9465.
4. Chanana, M.; Correa-Duarte, M. A.; Liz-Marzán, L. M. Insulin-Coated Goldnanoparticles: APlasmonic Device for Studying Metal-Protein Interactions. *Small* **2011**, *X*, 1–11.
5. Bharti, B.; Meissner, J.; Findenegg, G. H. Aggregation of Silica Nanoparticles Directed by Adsorption of Lysozyme. *Langmuir* **2011**, *27*, 9823–9833.
6. Chanana, M.; Rivera-Gil, P.; Correa-Duarte, M. A.; Liz-Marzán, L. M.; Parak, W. J. Physicochemical Properties of Protein-Coated Gold Nanoparticles in Biological Fluids and Cells before and after Proteolytic Digestion. *Angew. Chem., Int. Ed.* **2013**, *52*, 4179–4183.
7. Brewer, S. H.; Glomm, W. R.; Johnson, M. J.; Knag, M. K.; Franzen, S. Probing BSA Binding to Citrate-Coated Gold Nanoparticles and Surfaces. *Langmuir* **2005**, *21*, 9303–9307.
8. Zook, J. M.; MacCuspie, R. I.; Locasicio, L. E.; Halter, M. D.; Elliott, J. T. Stable Nanoparticle Aggregates/Agglomerates of Different Sizes and the Effect of Their Size on Hemolytic Cytotoxicity. *Nanotoxicology* **2011**, *5*, 517–530.
9. Schulze, C.; Kroll, A.; Lehr, C.-M.; Schäfer, U. F.; Becker, K.; Schnekenburger, J.; Isfort, C. S.; Landsiedel, R.; Wohlleben, W. Not Ready to Use - Overcoming Pitfalls when Dispersing Nanoparticles in Physiological Media. *Nanotoxicology* **2008**, *2*, 51–61.
10. Thanh, N. T. K.; Rosenzweig, Z. Development of an Aggregation-Based Immunoassay for Anti-Protein A Using Gold Nanoparticles. *Anal. Chem.* **2002**, *74*, 1624–1628.
11. Zook, J. M.; Rastogi, V.; MacCuspie, R. I.; Keene, A. M.; Fagan, J. Measuring Agglomerate Size Distribution and Dependence of Localized Surface Plasmon Resonance Absorbance on Gold Nanoparticle Agglomerate Size Using Analytical Ultracentrifugation. *ACS Nano* **2011**, *5*, 8070–8079.
12. Chah, S.; Hammond, M. R.; Zare, R. N. Gold Nanoparticles as a Colorimetric Sensor for Protein Conformational Changes. *Chem. Biol.* **2005**, *12*, 323–328.
13. Derjaguin, B. V.; Landau, L. The Theory of Stability of Highly Charged Lyophobic Sols and Coalescence of Highly Charged Particles in Electrolyte Solutions. *Acta Physicochim. URSS* **1941**, *14*, 633.
14. Verwey, E. J. W.; Overbeek, J. T. G. *Theory of the Stability of Lyophobic Colloids: The Interaction of Sol Particles Having an Electric Double Layer*; Elsevier: New York, 1948; pp 135ff.
15. Sevilla, P.; Sánchez-Cortés, S.; García-Ramos, J. V.; Feis, A. Concentration-Controlled Formation of Myoglobin/Gold Nanosphere Aggregates. *J. Phys. Chem. B* **2014**, *118*, 5082–5092.
16. Park, J. I.; Nguyen, T. D.; de Queirós Silveira, G.; Bahng, J. H.; rivastava, S.; Zhao, G.; Sun, K.; Zhang, P.; Glotzer, S. C.; Kotov, N. A. Terminal Supraparticle Assemblies from Similarly Charged Protein Molecules and Nanoparticles. *Nat. Commun.* **2014**, *5*, 3593.
17. Kalsin, A. M.; Grzybowski, B. A. Controlling the Growth of "Ionic" Nanoparticle Supracrystals. *Nano Lett.* **2007**, *7*, 1018–1021.
18. Sciortino, F.; Mossa, S.; Zaccarelli, E.; Tartaglia, P. Equilibrium Cluster Phases and Low-Density Arrested Disordered States: The Role of Short-Range Attraction and Long-Range Repulsion. *Phys. Rev. Lett.* **2004**, *93*, 055701.
19. Strozyk, M. S.; Chanana, M.; Pastoriza-Santos, I.; Pérez-Juste, J.; Liz-Marzán, L. M. Protein/Polymer-Based Dual-Responsive Gold Nanoparticles with pH-Dependent Thermal Sensitivity. *Adv. Funct. Mater.* **2012**, *22*, 1436–1444.
20. Kim, T.; Lee, C.-H.; Joo, S.-W.; Lee, K. Kinetics of Gold Nanoparticle Aggregation: Experiments and Modeling. *J. Colloid Interface Sci.* **2007**, *318*, 238–243.
21. Dixit, N. M.; Zukoski, C. F. Crystal Nucleation Rates for Particles Experiencing Short-Range Attractions: Applications to Proteins. *J. Colloid Interface Sci.* **2000**, *228*, 359–371.
22. Bharti, B.; Meissner, J.; Klapp, S. H. L.; Findenegg, G. H. Bridging Interactions of Proteins with Silica Nanoparticles: The Influence of pH, Ionic Strength and Protein Concentration. *Soft Matter* **2014**, *10*, 718–728.
23. Napper, D. H. *Polymeric Stabilization of Colloidal Dispersions*; Academic Press: New York, 1983; p 18ff.
24. Yang, W.; Sun, L.; Weng, J.; Chen, L.; Zhang, Q. Probing the Interaction of Bovine Haemoglobin with Gold Nanoparticles. *IET Nanobiotechnol.* **2012**, *6*, 26–32.
25. Röcker, C.; Pötzl, M.; Zhang, F.; Parak, W. J.; Nienhaus, G. U. A Quantitative Fluorescence Study of Protein Monolayer Formation on Colloidal Nanoparticles. *Nat. Nanotechnol.* **2009**, *4*, 577–580.
26. Glomm, W. R.; Halskau, O., Jr.; Hanneseth, A.-M. D.; Volden, S. Adsorption Behavior of Acidic and Basic Proteins onto Citrate-Coated Au Surfaces Correlated to Their Native Fold, Stability, and pI. *J. Phys. Chem. B* **2007**, *111*, 14329–14345.
27. Mortensen, N. P.; Hurst, G. B.; Wang, W.; Forster, C. M.; Nallathamby, P. D.; Retterer, S. T. Dynamic Development of the Protein Corona on Silica Nanoparticles: Composition and Role in Toxicity. *Nanoscale* **2013**, *5*, 6372–6380.
28. Brunauer, S.; Emmett, P. H.; Teller, E. Adsorption of Gases in Multimolecular Layers. *J. Am. Chem. Soc.* **1938**, *60*, 309–319.
29. Garabagiu, S. A. Spectroscopic Study on the Interaction Between Gold Nanoparticles and Hemoglobin. *Mater. Res. Bull.* **2011**, *46*, 2474–2477.
30. Zhang, D.; Neumann, O.; Wang, H.; Yuwono, V. M.; Barhoumi, A.; Perham, M.; Hartgerink, J. D.; Wittung-Stafshede, P.; Halas, N. J. Gold Nanoparticles Can Induce the Formation of Protein-Based Aggregates at Physiological pH. *Nano Lett.* **2009**, *9*, 666–671.

31. Smoluchowski, M. V. Drei Vorträge über Diffusion, Brownsche Bewegung und Koagulation von Kolloidteilchen. *Phys.Z.* **1916**, *17*, 557–585.
32. Evans, D. F.; Wennerström, H. *The Colloidal Domain*; Wiley-VCH: Weinheim, 1999; p 417ff.
33. Armstrong, J. K.; Wenby, R. B.; Meiselman, H. J.; Fisher, T. C. The Hydrodynamic Radii of Macromolecules and Their Effect on Red Blood Cell Aggregation. *Biophys. J.* **2004**, *87*, 4259–4270.
34. Verwey, E. J. W.; Overbeek, J. T. G. *Theory of the Stability of Lyophobic Colloids: The Interaction of Sol Particles Having an Electric Double Layer*; Elsevier: New York, 1948; pp 168ff.
35. Frens, G. Controlled Nucleation for the Regulation of the Particle Size in Monodisperse Gold Suspensions. *Nature Phys. Sci.* **1973**, *241*, 20–22.
36. Koppel, D. E. Analysis of Macromolecular Polydispersity in Intensity Correlation Spectroscopy: The Method of Cumulants. *J. Chem. Phys.* **1972**, *57*, 4814.